Available online at www.sciencedirect.com
SCIENCE DIRECT®
Digital Signal Processing 15 (2005) 4–18
Digital Signal Processing
www.elsevier.com/locate/dsp

Adaptive filter design for image deblurring by using multi-criteria blurred image information ☆

Ziya Telatar *

Faculty of Engineering, Department of Electronic Engineering, Ankara University, 06100 Besevler, Ankara, Turkey

Available online 11 September 2004

Abstract

This paper introduces a novel method to enhance the quality of blurred images. The proposed method is based on the estimation of the multi-criteria information of the degraded images. The multi-criteria information is extracted from the distribution model and the boundaries of the input image. The actual image blurred by an unknown distribution is correlated with predetermined reference models in order to choose the restoration filter model. The filter coefficient is then estimated using the edge information of the degraded image. Experiments have been conducted using simulated and real world images to evaluate the performance of the proposed method and the results are presented.

Keywords: Image enhancement; Image restoration; Distribution estimation; Image boundaries edge information

1. Introduction

Image blurring is a complex process resulted from the convolution of the original scenery and the blur function. Although all blurred images may look like a smoothed version of the original undistorted image, the degradation might be, in fact, resulted from a

☆ This work was supported by Ankara University, Scientific Research Projects (SRP-BAP), under Grant 2001-00-00-006.
* Fax: +90-312-223-23-95.
E-mail address: telatar@eng.ankara.edu.tr.

1051-2004/$ – see front matter
doi:10.1016/j.dsp.2004.07.003

variety of different phenomena such as motion, imperfections in the imaging system, and transmission/recording media. In classical restoration approaches, the blur model and its parameters are assumed to be known a priori and the degradation effect is reduced by basic techniques such as inverse filtering [1], blind deconvolution [1,3], and cepstrum [4,5]. The blur function that degrades the image, however, is generally unknown a priori for real-world images. In many applications, researchers desire and often require a higher quality image for their works [1,3,4]. Printing applications also require the use of better restoration to ensure that halftone reproductions of continuous images are of high quality [2]. It is then necessary to estimate the blur function model correctly to achieve better restoration.

Many of the recently published restoration algorithms assume that a Gaussian blur model degrades the image. Telatar and Tuzunalp [4,6] proposed a restoration algorithm based on the edge estimation of Gaussian blurred images. Molina et al. [7] suggested hyperparameter estimation on the basis of Bayesian and regularization methods using Gaussian noise assumption. Elad and Feuer [8] assumed a random noise hypothesis having a Gaussian distribution to establish an adaptive superresolution restoration filter. Ando and Hansuebsai [9] used a subjective evaluation method for restoration of color-faded images. Jalobeanu et al. [11], modeled the blur operator and the noise as Gaussian distributions in order to implement an hyperparameter estimation for simultaneous image restoration and they evaluated the performance of their algorithm using satellite images. With the assumption of Gaussian degradation, these methods have been applied to the problem with considerable improvement.

Although the Gaussian assumption is valid for some kind of applications, there are, however, instances where this assumption limits the applicability of the methods. Various phenomena such as the atmosphere, motion, X-rays, and medical imaging systems, introduce degradation other than Gaussian blur. The use of the same blur model for all these different scenarios will result in a performance loss in the restoration process.

A number of different distribution models such as Gaussian, Poisson, etc. have been introduced to define the image degradation process [10]. However, to achieve further improvement for a broader range of restoration applications, a more robust restoration algorithm is needed. Instead of using a fixed assumption for all different cases of blurring processes, the most suitable restoration filter has to be estimated for each individual scenario for a better performance. Although the probability density curves for most distribution types are similar to each other, they produce distinct results in the restoration process depending on their filter model. Therefore, the reliability of the filter model must be tested in terms of distribution hypothesis to choose a better filter model and to obtain more robust restoration results. There are several hypothesis test method in the literature to test whether the distribution is Gaussian [12–14] or not. We shall not discuss any of these special tests here, but rather use some properties of chi-square test to estimate the distribution model.

This paper proposes a new, multi-criteria based restoration algorithm. The proposed method is a two-stage process. In the first stage, a blur model estimation method is applied to the degraded input image to estimate the blur distribution. At this stage, some predefined models are tried to decide the most suitable degradation model. In the second stage, blur filter coefficient is searched iteratively based on the edge points within the image.

The paper is organized as follows; Section 2 introduces general image degradation model and filter model estimation procedure with some distributions related to the degra-

dation models of images. Section 3 presents the filter coefficient estimation from the filter model defined and the restoration algorithms. Section 4 presents some experimental results. Finally, Section 5 presents the concluding remarks.

2. Image degradation and distribution models

2.1. General image degradation

A standard description of the image degradation model is given as a transformed form of an original scene as follows:

$$y = Hx + n, \tag{1}$$

where the original image x has been degraded by the blur matrix H and additive noise n. Additive noise can be resulted from electronic components of the imaging system or the channel which is independent from the original image x. The statistics of the additive noise can be measured or known from the previous experiments. Thus, the additive noise component may be removed from the degraded image by using basic image processing techniques in signal domain [1,3,4]. In this study, we focus on the blur degradation model only and leave out the additive noise problem and refer the reader to Refs. [1,4,6] for further details. Discarding the additive noise component, Eq. (1) can be rewritten as

$$y = Hx. \tag{2}$$

Equation (2) states that the degradation is the result of a convolution between the original scenery and the blur function.

2.2. Blur distribution models

The blur function $h(n_1, n_2)$ representing the blur matrix H can be from different statistical distributions as mentioned in Section 1 and different blur models can be identified for each distribution. In traditional image restoration applications, the blur model is assumed to be Gaussian as it is a more general form [1–9] and it covers all other distributions. Unfortunately, this assumption is not valid for all types of degradations, as the origin of blur process can be different for various applications. In this study, blur distribution model affecting the input image is estimated and this estimation is correlated with a number of predefined reference models. The model that fits better to the observed data is chosen for restoration. Basic distribution models encountered in image formation process [10] are listed below:

- *Poisson distribution*. In the area of astronomical imaging, X-rays, mammogram and digital angiographic imaging, the degradation can often be characterized by Poisson distribution which is modeled as

$$h_{\mathrm{R}(1)}(n_1, n_2; \lambda_1, \lambda_2) = \frac{\lambda_1^{n_1}\lambda_2^{n_2}}{(n_1)!(n_2)!}e^{-(\lambda_1+\lambda_2)}. \tag{3}$$

- *Exponential distribution*. This degradation model is encountered in some laser based imaging applications and can be characterized as

$$h_{\mathrm{R}(2)}(n_1, n_2) = e^{-n_1^2+n_2^2}. \tag{4}$$

- *Gaussian distribution*. This model is the most common model and most of the applications such as atmospheric turbulence, unfocused camera, motion, etc., are characterized by this distribution. The model for Gaussian distribution is given as

$$h_{\mathrm{R}(3)}(n_1, n_2) = \frac{1}{2\pi\sigma^2} e^{-(n_1^2+n_2^2)/2\sigma^2}. \tag{5}$$

- *Rayleigh distribution*. This distribution model, which is quite similar to the Gaussian distribution, is encountered in some medical imaging and remote sensing (like astronomical imaging) applications. The distribution is modeled as

$$h_{\mathrm{R}(4)}(n_1, n_2; \sigma^2) = \frac{n_1 n_2}{\sigma^4} e^{-(n_1^2+n_2^2)/2\sigma^2}, \tag{6}$$

where n_1 and n_2 are dimensions of the blur kernel, σ^2 is the variance of the blur function, parameter λ is the rate of occurrence, and h_{R}'s are distribution models for the related blur functions in two dimension. Although the given distributions are the most common ones encountered in practical applications, other distribution models can be included into the list of the distributions as required. These distribution models are tested during the blur function estimation procedure in order to decide the distribution model of the blur. The estimated blur function model defines the restoration filter model that will be used with the notation of h_{f} throughout the paper.

2.3. Estimation of the blur filter model

In this work, chi-square test is utilized to estimate the distribution model of the degraded image. The chi-square test is the most commonly used procedure for evaluating distributional assumptions [12–14]. The major advantage of the chi-square test is its versatility as it can easily be applied to any distribution without requiring the values of the distribution parameters [12]. The test procedure requires n samples of the observed data whose probability density function is unknown. The frequency distribution of the observed data is calculated using k frequency bins. The expected frequency of the hypothesized probability distribution is also calculated. A comparison between the observed and the hypothesized distributions is made and a test statistic is calculated as below:

$$\chi^2 = \sum_{i=1}^{k} \frac{(\alpha_i^j - \beta_i)^2}{\beta_i}, \quad j = 1, \ldots, N_{\mathrm{m}}, \tag{7}$$

where α_i is the frequency distribution of the observed data, β_i is the frequency distribution of the hypothesized probability density function, k is the number of frequency bins, and N_{m} is the number of distribution models which, in our case, is 4. The test statistic tends to exceed a chi-square variate if the assumed model does not fit the observed data. The values of χ^2 falls between zero and infinity. It is clear that the more "unusual" the observed distribution gets, the higher the estimation result is; whereas if the observed samples matches perfectly to the expected ones, then χ^2 becomes zero.

In Fig. 2, a block diagram for proposed distribution estimation algorithm is shown. In this figure, "distribution models block" stores a number of predefined distribution models. "Distribution test block" compares the distribution curve of each model with the input image distribution curve computed by the "input image distribution block." The model decision block decides the best fitting distribution model for the degraded input image after testing for all hypothesizes. The estimated distribution model defines the filter model, which is obtained from the output of "distribution test block" (filter model block). The distribution model estimations process is summarized in the following algorithm:

(1) Define the model parameters of assumed distribution represented by h_{R}.
(2) Divide the data presented in step 1 into k frequency bins (or cells) and determine the probability of a random value from the assumed model falling within each cell. The bounds of a cell are defined as

$$Pr\ (M_i \leqslant h_{\mathrm{R}}\ (\text{and } y) < N_i), \quad i = 1, \ldots, k, \tag{8}$$

where M_i and N_i denote the lower and upper bounds of ith frequency bin.
(3) Multiply each of the bin probabilities by the sample size n. This yields the expected number of observations for each bin under the assumed model (β_i).
(4) Read the observed data y which is input image in our case.
(5) Repeat step 1 to step 4 for observed data.
(6) If the observed data are not initially tabulated, count the number of observed values in each class. Denote this number as α_i.
(7) Calculate the χ^2 value according to Eq. (7) between the unknown image (observed data) and the reference distribution data.
(8) Compare the computed χ^2 value with the curves given in Fig. 1 in order to decide the best fitting distribution. High values of χ^2 signify that the observed data contradicts the assumed model.

The degraded image and the distribution test models are classified into 20 bins each of which defining a specific interval for gray levels. The number of pixels falling into each

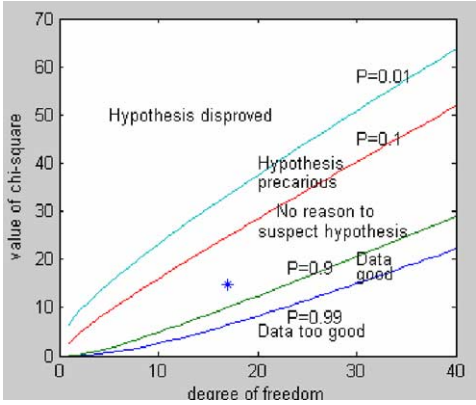

Fig. 1. Chi-square goodness of fit test evaluation regions.

interval are counted and correlated with each other according to Eq. (7). Consequently, the degree of freedom required for defining the exact place of χ^2 on graphical representation is calculated as 17 by taking into account the parameters of distribution such as standard deviation, mean and kernel (Degree of freedom $= s - 3$, s is the number of bins or cells.) After the steps given above, the algorithm produces a result for estimated distribution as shown in Fig. 1. The curves in Fig. 1 have been calculated using the standard tables [12–14]. If the star mark falls between the probability curves of $P = 0.1$ and $P = 0.9$, the hypothesis is accepted, i.e., the observation is assumed to be from the tested distribution. If the star is above the curves, the hypothesis is "precarious" or "disproved." If the star is under the curves, the result is interpreted as data is "good" or "too good."

3. Estimation of the filter model coefficient and restoration algorithm

3.1. Filter model coefficient estimation

The restoration algorithm estimates the distributional curve of degraded image on the basis of the above given method, and then decides the filter model from the output of the distribution test block given in Fig. 2 according to Eqs. (3)–(6). The next step is to estimate the filter parameters and the filter coefficients.

In this study, gradient edge detection method [1,4] is used to estimate the filter coefficient. High frequency regions in the image, called edge pixels, are spread over the neighborhood pixels causing the loss of the details in blurred images. Thus, the edge map of degraded images does not contain more edge lines or points than the original image. The edge map of an image represents important information about the degradation.

Figure 2 shows the filter model coefficient estimation procedure from the edge information of the degraded image. This iterative process is given as follows:

Step 1. Define the filter model parameters h_{f} on a basis of estimated filter model h_{R} (filter model block in Fig. 2).
Step 2. Find the edge map of the actual image, ∇y (∇ is the gradient operator [1]).
Step 3. Calculate the number of edges in edge map

$$\delta_n = \sum\sum(\nabla y) \geqslant p. \tag{9}$$

Step 4. Assign a filter coefficient for the calculated number of edges (filter coefficient estimation block in Fig. 2)

$$\gamma_n = F(\delta_n), \quad (\gamma\text{—filter coefficient}). \tag{10}$$

Step 5. Construct a restoration filter using the parameters defined in step 1 and the filter coefficient calculated in step 4 (restoration filter block in Fig. 2).
Step 6. Restore the image according to Eq. (17) (image transform, filtering, inverse transform block in Fig. 2) in order to obtain y_{new}.
Step 7. Find edges of output image obtained from step 6 and calculate the number of edges again

$$\gamma_{n+1} = \sum\sum(\nabla y_{n+1}) \geqslant p. \tag{11}$$

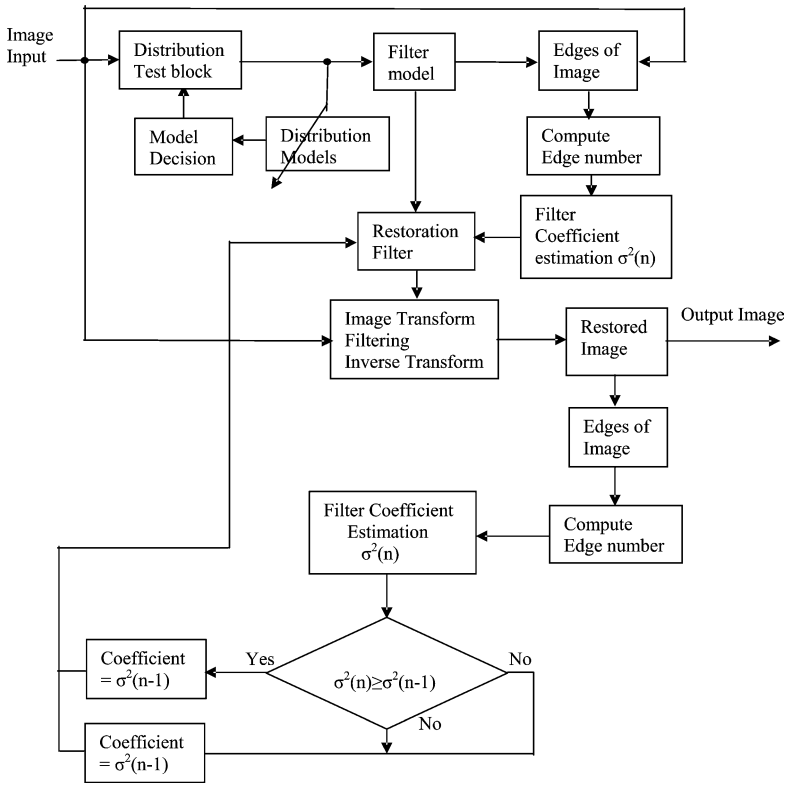

Fig. 2. General block diagram of the image restoration system.

Step 8. Assign a new filter coefficient value for step 7

$$\gamma_{n+1} = F(\gamma_{n+1}). \tag{12}$$

Step 9. Compare the number of edges in step 7 with the previously calculated number of edges

$$e = \gamma_{n+1} - \gamma_n \tag{13}$$

if

$$\gamma_{n+1} = \begin{cases} \gamma_{n+1}, & e > 0, \\ \gamma_n, & e \leqslant 0. \end{cases}$$

Step 10. Assign the next value for the filter coefficients and repeat the steps from 5 to 10. Iteration steps is increased as follows:

$$b^{i+1} = b^i + \Delta b^i \big[n_1(i+1);\ n_2(i+1)\big], \tag{14}$$

where b^{i+1} is the convergence vector of iterations, Δb^i is the iteration step size.

Step 11. Restore the image by the filter with final coefficients estimated.

After a certain number of iterations, the best edge map with the highest number of calculated edges is determined and the filter coefficient is set as the number of edges in this image. This coefficient is used to design final restoration filter in step 11 (Note that different filter coefficients are searched for a fixed blur kernel size, and then kernel size is changed.)

$$\gamma = f(\nabla) = \left\{ \sum\sum \left[\nabla y(n_1; n_2) \geqslant p \right] \right\}_{\max}. \tag{15}$$

Restoration filter coefficients are estimated by the gradient-based edge computations in which Sobel operator is involved in the gradient calculations. Mathematical representations of gradient based edge detection is well defined in the literature [1].

The choice of the threshold level for the edge points is particularly important, as an improper choice of this level may cause the detection algorithm to make a false trigger. To prevent false triggers, a fixed threshold level (p) is introduced and then the upper level of threshold is accepted as an edge point. If p is too low, noise may be detected as an edge point. If p is too high, some edge points may not be detected. Thus, the threshold level p has been taken as 35% of the amplitude of the maximum edge pixel level.

Figure 4 shows the result of the filter parameter estimations. Figures 4a, 4b, and 4c show the number edge points (vertical axes) versus filter parameter (horizontal axes scaled by 10). The maximum numbers of edge points (peak values shown in figures) are chosen as the best filter parameter for the restoration algorithm.

3.2. Restoration

Having estimated the filter model parameter and the coefficient, Fourier domain Cepstrum transform is used for filtering. The Cepstrum algorithm has been extensively used for image processing applications and its features are well documented in the literature [1,4–6]. Fourier domain Cepstrum transform of Eq. (2) is given as

$$\hat{Y} = \hat{X} + \hat{H}. \tag{16}$$

Equation (16) shows that blurred image is decomposed into a sum of original scenery of the image component and blur model component. If the estimated filter model is $h_{\mathrm{f}}(n_1, n_2)$ after the iterations, the filtering is realized in Cepstrum domain as follows:

$$\hat{Y}_{\mathrm{new}} = \hat{X} + \hat{H} - \hat{H}_{\mathrm{f}}. \tag{17}$$

By minimizing the error between the blur function model coefficients and the constructed filter model coefficients, an improvement in the image quality is achieved. For the simulated images, improvement in the image quality (ISNR) is defined as

$$\mathrm{ISNR} = 10 \log_{10} \sum\sum \left(\frac{[x - y]^2}{[x - y_{\mathrm{new}}]^2} \right), \tag{18}$$

where $x(n_1, n_2)$, $y(n_1, n_2)$, and $y_{\mathrm{new}}(n_1, n_2)$ are the original, degraded and restored images respectively. However, ISNR metric cannot be applied to the real world images as the undegraded original image is unavailable in the process. For that reason IMPR metric is

defined in order to evaluate the improvement in the image quality for real world degraded images as

$$\mathrm{IMPR} = 10\log_{10}\frac{[\sum\sum|y|]^2}{[\sum\sum|y| - \sum\sum|y_{\mathrm{new}}|]^2}, \tag{19}$$

where $y(n_1, n_2)$ and $y_{\mathrm{new}}(n_1, n_2)$ are degraded and restored images, respectively.

4. Experimental results

The performance of the proposed restoration algorithm has been evaluated using a 200×200 pixel artificial test image, the camera man image, the Taj Mahal image, the child image, an astronomical image, the car racing image (a motion image), and a medical image. Experimental results are discussed in this section.

The first image used to test the algorithm is shown in Fig. 3a. This image, which is an artificially generated 256 gray level image, is degraded by Gaussian distributed blur function. Normalized intensity levels of pixels (between 0 and 1) for the degraded image are placed into one of 20 equally divided bins depending on their pixel values. The same procedure is applied for the test distributions. The number of pixels falling into each class is calculated for both degraded image and distribution test model and they are correlated using the chi-square test given in Eq. (7). Figure 3b shows the result for a Poisson test model. In this case, χ^2 value is calculated as 48.16 and the hypothesis is disproved (the star is outside the acceptance region). The Rayleigh and the exponential distribution models result in χ^2 values of 28.18 and 742.07, respectively. The star falls outside the acceptance region for these distributions models and hypothesizes are rejected. When the correct distribution model, which is Gaussian model for this case, is tested, the star stays inside the acceptance region as shown in Fig. 3c ($\chi^2 = 14.66$) and the hypothesis is accepted. ISNR and IMPR calculations in case of the correct filter estimation are obtained as 253.49 and 311.67 dB, respectively (for additive noise free case). Note that incorrect distribution estimation results given above are only used to show the correctness of the distribution hypothesis simulations.

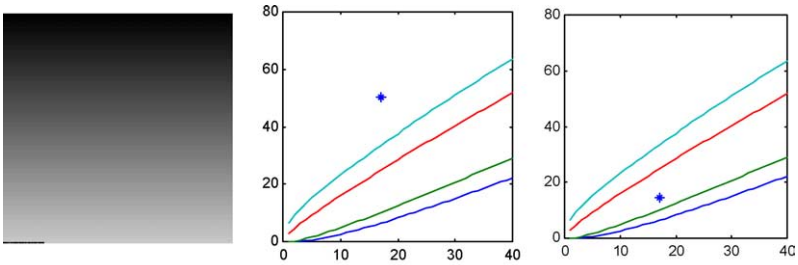

Fig. 3. (a) 256 gray level test image, (b) test result for original undegraded image in (a), (c) test result for Gaussian degraded form of (a).

After establishing the restoration filter model from the estimated distribution information, the proposed algorithm is used to estimate the filter coefficient from the edge information of the degraded image. The images in Figs. 5, 6, and 7 are degraded by different distribution models with filter coefficient of 3.6. The filter coefficient is estimated by the algorithm for each degradation scenario and the results are shown in Table 1. Figures 4a, 4b, and 4c show the edge estimation results during the iterations. The calculated maximum edge number is related to the restoration filter coefficient. In Figs. 5a and 5b, Gaussian blurred images of Taj Mahal and its edge map in which image details have been lost are shown. Figure 5c shows the restored images resulted from not using the proper

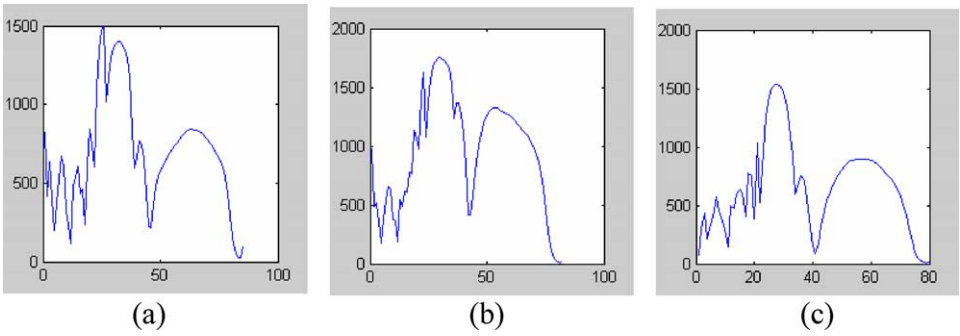

Fig. 4. Filter coefficient estimation results by edge information. (a) Result from Fig. 5a, (b) result from Fig. 6a, (c) result from Fig. 7a.

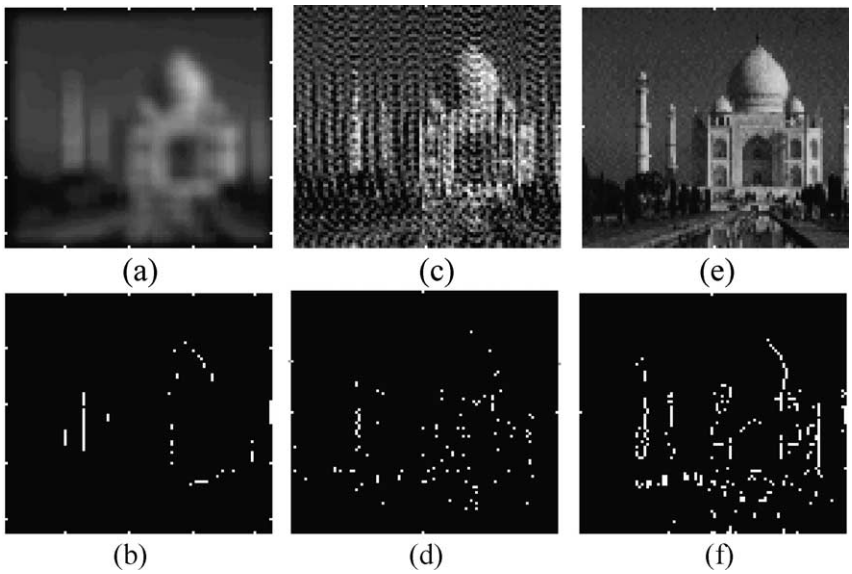

Fig. 5. (a) Blurred Taj Mahal image with variance of 3.6 and blur kernel of 15, (b) edge map of (a), (c) restored image by the filter estimated incorrectly from the degraded image (variance 3), (d) edge map of (b), (e) resulting restored image from (a), (f) edge map of resulting image.

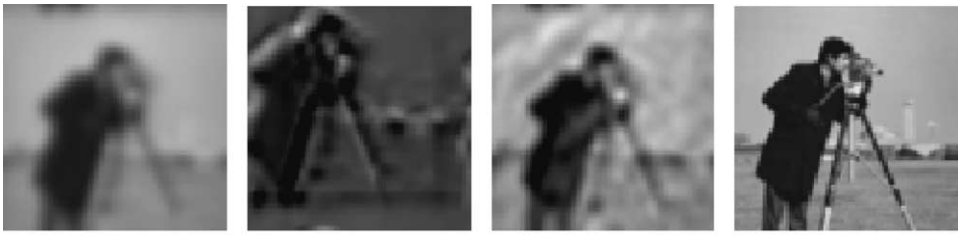

Fig. 6. (a) Camera man image blurred by Rayleigh distribution, (b) restored image by Poisson estimated filter model, (c) restored image by Gaussian estimated filter model, (d) restored image by Rayleigh estimated filter model (correct estimation).

Fig. 7. (a) Gaussian degraded child image, (b) restored image from (a) by Poisson filter, (c) restored image from (a) by exponential filter, (d) restored image from (a) by Gaussian filter.

filter model and coefficient. Figure 5d shows the edge map of the image in Fig. 5c. Because of the erroneous restoration, the resulting image is not clear. Figures 5e and 5f are the restored image and its edge map for the correctly estimated filter model (Gaussian) and filter coefficient of 3.60 with an improvement in image quality of ISNR = 196.95 and IMPR = 301.93 as given in Table 1. The Taj Mahal image has also been degraded with the Poisson filter and the same procedure has been repeated. The numerical results of the restoration are given in Table 1 together with the improvements in image quality.

The camera man image shown in Fig. 6a is a Rayleigh degraded image. Figures 6b and 6c shows the results of the restoration using a Poisson and Gaussian distributed blurs, respectively. Blurred image cannot be restored efficiently as the chosen restoration models are incorrect. Figure 6d shows the result of using the correct blur model (Rayleigh) with a filter coefficient of 3.65. The calculated ISNR value is 29.14 dB and IMPR value is 36.99 dB as shown in Table 1.

As an another example, the algorithm has been applied to the child image shown in Fig. 7 and similar restoration results have been obtained for three different scenarios (for Poisson, exponential, and Gaussian degraded inputs). Figures 7a, 7b, and 7c show Gaussian degraded input image, restoration result by using Poisson filter (incorrect estimation), and restoration result by using exponential filter (incorrect estimation), respectively. Again, Fig. 7d is a result of a correct distribution estimation from Gaussian degraded image with the improvement in image quality of 205.08 dB for ISNR and 288.97 dB for IMPR calcu-

Table 1
Distribution (also filter model) estimation and restoration results for simulated images

Images	Blurred with	Distribution test model	Test result (χ^2)	Estimated restoration filter type	Estimated filter coefficient	ISNR	IMPR
Fig. 3, 256 gray level test image	Gaussian	**Gaussian**	**14.66**	**Gaussian**	**3.61**	**25.67**	**62.59**
		Poisson	48.16	Poisson	7.73	−59.43	16.33
		Rayleigh	28.18	Rayleigh	8.81	−7.89	8.27
		Exponential	742.07	Exponential	10.0	−6.01	2.26
Fig. 5, Taj Mahal (256 × 256)	Gaussian	**Gaussian**	**14.27**	**Gaussian**	**3.60**	**196.95**	**301.93**
		Poisson	224.56	Poisson	6.74	−54.66	32.50
		Rayleigh	36.44	Rayleigh	6.00	8.29	22.13
		Exponential	1.42×10^4	Exponential	9.98	−3.38	2.27
Fig. 5, Taj Mahal (256 × 256)	Poisson	Gaussian	218.33	Gaussian	5.96	−1.97	0.04
		Poisson	**13.87**	**Poisson**	**3.64**	**31.56**	**11.12**
		Rayleigh	35.63	Rayleigh	5.00	0.04	16.67
		Exponential	1.46×10^4	Exponential	8.20	−0.02	1.11
Fig. 6, camera man (70 × 70)	Exponential	Gaussian	28.23	Gaussian	9.98	7.65	37.18
		Poisson	38.96	Poisson	5.40	1.09	24.13
		Rayleigh	30.53	Rayleigh	4.76	−0.52	27.29
		Exponential	**17.02**	**Exponential**	**3.63**	**52.82**	**40.64**
Fig. 6, camera man (70 × 70)	Rayleigh	Gaussian	10.59	Gaussian	2.38	−55.29	0.051
		Poisson	34.44	Poisson	6.25	−58.47	19.01
		Rayleigh	**6.48**	**Rayleigh**	**3.65**	**29.14**	**36.99**
		Exponential	38.93	Exponential	9.00	−7.53	1.46
Fig. 7, child (200 × 200)	Rayleigh	Gaussian	28.17	Gaussian	2.31	−66.29	0.02
		Poisson	125.47	Poisson	6.53	−6.176	19.86
		Rayleigh	**18.25**	**Rayleigh**	**3.62**	**241.62**	**37.67**
		Exponential	336.48	Exponential	9.27	−10.08	1.71
Fig. 7, child (200 × 200)	Gaussian	**Gaussian**	**14.66**	**Gaussian**	**3.60**	**205.08**	**288.97**
		Poisson	135.49	Poisson	8.36	−58.47	27.82
		Rayleigh	27.30	Rayleigh	5.42	4.78	28.12
		Exponential	102.04	Exponential	9.46	−6.64	1.88

lations. The filter coefficient estimation result has been shown in Fig. 4c for this case. The other numerical estimation and restoration results for Fig. 7 are given in Table 1.

Algorithm has also been evaluated with real-world degraded (not simulated) images. Figure 8a shows an original medical image obtained from ultrasonography in which the image is degraded by motion. After applying the algorithm to this image, the blur distribution on the image has been estimated as Gaussian. The image restored by the presented algorithm is shown in Fig. 8b with an IMPR improvement of 43.13 dB as given in Table 2. In Fig. 9a another degraded real image is shown. The proposed algorithm estimates the degradation as Gaussian with $\chi^2 = 5.48$. The restored image is shown in Fig. 9b and the improvement in image is calculated as IMPR = 34.82 dB. In Fig. 10a a car racing image is shown. The image is degraded by motion effect during imaging process. The blur degradation model is estimated as Poisson. The restored image is shown in Fig. 10b. The improvement in image quality is IMPR = 20.06 dB. The last image (Fig. 11a, Spiral

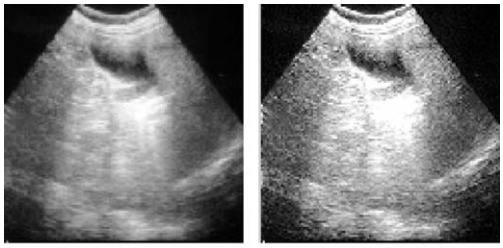

Fig. 8. (a) Originally degraded medical image, (b) restored image from (a) image.

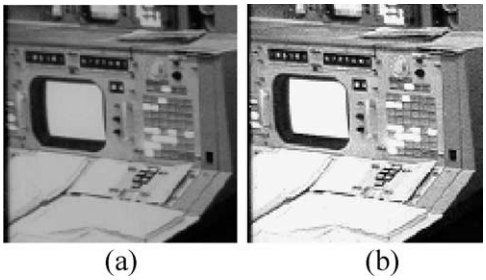

Fig. 9. (a) Originally degraded real world, (b) restored image from (a).

Table 2
Distribution (and filter model) estimation and restoration results for real-world images

Images	Estimated restoration filter type	Test result (χ^2)	Estimated filter coefficient	Improvement IMPR (dB)
Fig. 8,	**Gaussian**	**0.43**	**4.72**	**43.13**
(212 × 212)	Poisson	3.05×10^3	6.97	−4.87
	Rayleigh	2.15	4.69	31.03
	Exponential	1.58×10^3	5.89	−5.16
Fig. 9,	**Gaussian**	**5.48**	**4.70**	**34.82**
(256 × 256)	Poisson	9.70×10^3	5.06	−5.55
	Rayleigh	23.35	9.26	16.96
	Exponential	1.26×10^3	4.99	−12.92
Fig. 10,	Gaussian	5.43×10^3	2.91	12.32
(200 × 200)	**Poisson**	**4.47**	**4.61**	**20.06**
	Rayleigh	20.27	2.23	12.84
	Exponential	5.43×10^3	4.24	12.77
Fig. 11,	Gaussian	22.21	5.50	26.40
(280 × 280)	Poisson	1703.16	3.21	−5.54
	Rayleigh	**8.73**	**2.62**	**34.77**
	Exponential	1.58×10^4	2.51	−37.65

Galaxy) evaluated in this paper is an astronomical image taken by Hubble space telescope. The degradation in this image is estimated as Rayleigh distributed blur. The restored image is shown in Fig. 11b. The improvement in image quality is IMPR = 34.77. The improve-

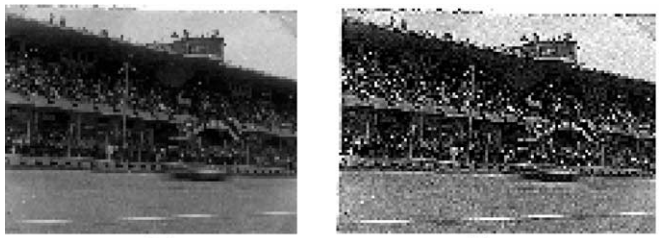

Fig. 10. (a) Originally degraded car racing image, (b) restored image from (a).

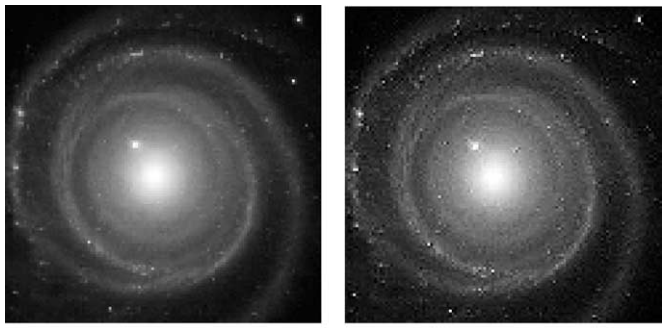

Fig. 11. (a) Originally degraded astronomical image (Spiral Galaxy image taken by HST), (b) restored image from (a).

ment results are summarizes in Table 2. The negative improvement values in Table 2 indicated that there is an extra degradation in image or no improvement is achieved in image quality.

5. Conclusion

This paper proposes a restoration algorithm based on the estimation of the multi-criteria image information such as blur model and filter coefficient. Basic distribution models that are common to many image degradation processes have been examined for restoration. After deciding the restoration filter model by comparing the curves of distribution models to the input image distribution curve, the algorithm estimates the filter coefficient from the edge information of the degraded image. Restoration is successfully realized by the filter, resulting in improved the image quality.

Experimental results presented in this paper show that a better restoration requires estimation of the degradation distribution model and restoration filter coefficient together. Other distribution models can be included in the algorithm as required.

References

[1] J.S. Lim, Two-Dimensional Signal and Image Processing, Prentice Hall, 1990.
[2] S. Hein, A. Zakhor, Half-tone to continuous-tone conversion of error-diffusion coded images, IEEE Trans. Image Proc. 4 (1995) 208–216.
[3] S.C. Pohlig, New techniques for blind deconvolution, Opt. Eng. 20 (1981) 281.
[4] Z. Telatar, O. Tuzunalp, Edge estimation and restoration of Gaussian degraded images, JIST J. Image Sci. Technol. 42 (4) (1998) 370–374.
[5] J.K. Lee, M. Kabrisky, M.E. Oxley, S.K. Rogers, D.W. Ruck, The complex Cepstrum applied to two-dimensional images, Pattern Recogn. 26 (1993) 1579–1592.
[6] Z. Telatar, Adaptive restoration of blurred satellite image, ISI 51st Session of the International Statistical Institute, vol. 2, 1997, pp. 499–500.
[7] R. Molina, A.K. Katsaggelos, J. Mateos, Bayesian and regularization methods for hyperparameter estimation in image restoration, IEEE Trans. Image Proc. 8 (2) (1999) 231–246.
[8] M. Elad, A. Feuer, Superresolution restoration of an image sequence: Adaptive filtering approach, IEEE Trans. Image Proc. 8 (3) (1999) 387–395.
[9] Y. Ando, A. Hansuebsai, K. Khantong, Digital restoration of faded color images by subjective method, J. Image Sci. Technol. 41 (1997) 259–265.
[10] M.R. Banham, A.K. Katsaggelos, Digital image restoration, IEEE Signal Process. Mag. 14 (2) (1997) 24–41.
[11] A. Jalobeanu, L. Blanc-Feraud, J. Zerubia, Hyperparameter estimation for satellite image restoration using a MCMC maximum-likelihood method, Pattern Recogn. 35 (2002) 341–352.
[12] G.J. Hahn, S.S. Shapiro, Statistical Models in Engineering, Wiley, 1994.
[13] A.V. Metcalfe, Statistics in Engineering, Chapman & Hall, 1994.
[14] J.P. Noonan, H.M. Polchlopek, A hypothesis testing technique for the wavelet transform in the presence of noise, Digital Signal Process. 3 (1993) 89–96.

Ziya Telatar received the BSc degree in electronics and telecommunications engineering from Yildiz Technical University, Turkey, in 1983, the MSc degree in electronics engineering from Ankara University, in 1993, and the PhD degree in electronics engineering from Ankara University, Turkey, in 1996. Dr. Telatar joined the Department of Electronics Engineering at Ankara University in 1990, where he is currently working as Assistant Professor and second Chairman. His research interests include image restoration, recognition, motion estimation, biomedical signal, and image processing.